broadly neutralizing antibody VRC03, which was one of two antibodies we isolated along with VRC01 (*12*). Meanwhile, three residues are provided by the CDR L3—$Tyr91_{VRC01}$, $Glu96_{VRC01}$, and $Phe97_{VRC01}$—with a combined interaction surface of 190 $Å^2$ (tables S3 and S13). These three residues lie at the junction between V and J genes. They make important hydrophobic interactions with loop D of gp120, and two of them are conserved between VRC01 and VRC03. Although it is difficult to know how precisely the CDR L3 needs to be aligned, with only three contact residues variation at the $V_κ$-J gene junction should provide sufficient diversity for it to be represented in the repertoire.

33. R. W. Sanders *et al*., *J. Virol.* **76**, 7293 (2002).
34. D. A. Calarese *et al*., *Science* **300**, 2065 (2003).
35. G. Ofek *et al*., *J. Virol.* **78**, 10724 (2004).
36. B. F. Haynes *et al*., *Science* **308**, 1906 (2005).
37. C. Berek, A. Berger, M. Apel, *Cell* **67**, 1121 (1991).
38. Analysis of the HIV-1 Env-reactive antibody repertoire from infected individuals shows increased levels of affinity maturation (*30*). Analysis of a subset of this data (appendix S1) containing 147 heavy and 147 light chains from HIV-1 Env-reactive antibodies reveals an average of 15 alterations (30 maximum) for the heavy chain and an average of 8.6 alterations (22 maximum) for the light chain (fig. S13). In terms of the subset of HIV-1 Env-reactive antibodies that are broadly neutralizing (such as 2G12, 2F5, 4E10, and b12), antibodies b12 and 2G12 have 45 and 51 changes, respectively, relative to nearest genomic precursors in their V_H and J segments of the heavy chain (*31*).
39. Similar significant reductions in affinity have been observed with reversion of other broadly neutralizing antibodies to HIV-1 to putative genomic sequences (*47*–*49*); these observations have led to the suggestion that the dramatically reduced germline affinity for gp120 might hinder the initiation of affinity maturation of these antibodies (*50*). That is, if the affinity for gp120 of the genomic precursor of a broadly neutralizing antibody were below the threshold required for the nascent B cell to mature, then maturation would either not occur or would need to occur in response to a different immunogen. This lack of guided initiation of the maturation process may provide an explanation for the absence of such broadly neutralizing antibodies in the first few years of infection. Conversely, the introduction of modified gp120s with affinity to genomic precursors and affinity maturation intermediates could provide a mechanism by which to elicit antibodies like VRC01.
40. M. G. Rossmann, *J. Biol. Chem.* **264**, 14587 (1989).
41. T. J. Smith, E. S. Chase, T. J. Schmidt, N. H. Olson, T. S. Baker, *Nature* **383**, 350 (1996).
42. D. Corti *et al*., *PLoS ONE* **5**, e8805 (2010).
43. J. P. Anderson *et al*., *J. Virol.* **74**, 10752 (2000).
44. E. J. Dodson, M. Winn, A. Ralph, *Methods Enzymol.* **277**, 620 (1997).
45. M. L. Connolly, *J. Mol. Graph.* **11**, 139 (1993).
46. D. G. Myszka *et al*., *Proc. Natl. Acad. Sci. U.S.A.* **97**, 9026 (2000).
47. X. Xiao, W. Chen, Y. Feng, D. S. Dimitrov, *Viruses* **1**, 802 (2009).
48. X. Xiao *et al*., *Biochem. Biophys. Res. Commun.* **390**, 404 (2009).
49. M. Pancera *et al*., *J. Virol.* **84**, 8098 (2010).
50. D. S. Dimitrov, *MAbs* **2**, 347 (2010).
51. T.Z., I.G., Z.Y., J.S., L.S., G.J.N., J.R.M., and P.D.K. designed the research; T.Z., I.G., X.W., Z.Y., K.D. A.F., W.S., L.X., Y.Y., and J.Z. performed the research; X.W., Y.K., J.F.S., M.C.N., and J.R.M. contributed new reagents or reference data; T.Z., I.G., X.W., J.S., L.S., G.J.N., J.R.M., and P.D.K. analyzed the data; and T.Z., I.G., J.S., L.S., G.J.N., J.R.M., and P.D.K. wrote the paper, on which all authors commented. We thank I. A. Wilson and members of the Structural Biology Section and Structural Bioinformatics Core, Vaccine Research Center, for discussions and comments on the manuscript; the staff of sector 22 for assistance with data collection; and J. Stuckey for assistance with figures. Support for this work was provided by the Intramural Research Program of NIH and by grants from NIH and from the International AIDS Vaccine Initiative's Neutralizing Antibody Consortium. Use of sector 22 (Southeast Region Collaborative Access team) at the Advanced Photon Source was supported by the U.S. Department of Energy, Basic Energy Sciences, Office of Science, under contract W-31-109-Eng-38. Coordinates and structure factors for the VRC01-gp120 complex have been deposited with the PDB under accession code 3NGB.

Supporting Online Material

www.sciencemag.org/cgi/content/full/science.1192819/DC1
Materials and Methods
Figs. S1 to S16
Tables S1 to S14
References
Appendix S1

25 May 2010; accepted 1 July 2010
Published online 8 July 2010;
10.1126/science.1192819
Include this information when citing this paper.

Gamma-Ray Emission Concurrent with the Nova in the Symbiotic Binary V407 Cygni

The Fermi-LAT Collaboration*†

Novae are thermonuclear explosions on a white dwarf surface fueled by mass accreted from a companion star. Current physical models posit that shocked expanding gas from the nova shell can produce x-ray emission, but emission at higher energies has not been widely expected. Here, we report the Fermi Large Area Telescope detection of variable γ-ray emission (0.1 to 10 billion electron volts) from the recently detected optical nova of the symbiotic star V407 Cygni. We propose that the material of the nova shell interacts with the dense ambient medium of the red giant primary and that particles can be accelerated effectively to produce $π^0$ decay γ-rays from proton-proton interactions. Emission involving inverse Compton scattering of the red giant radiation is also considered and is not ruled out.

V407 Cygni (V407 Cyg) is a binary system consisting of a Mira-type pulsating red giant (RG) with a white dwarf (WD) companion; these properties place it among the class of symbiotic binaries (*1*). Though one of the more active symbiotic systems, V407 Cyg has historically shown an optical spectrum in quiescence dominated by the Mira-like RG (M6 III) and only weak emission lines [see, for example, (*2*)]. Its infrared continuum (consistent with a dusty wind) and maser emission (*3*) are detected at levels similar to other symbiotic Miras [for instance, R Aqr (*4*)]. One outstanding anomaly of V407 Cyg is a strong Li I λ6707 line indicative of an overabundance of Li relative to normal Mira RGs (*5*, *6*). Based on the 745-day pulsation period of the RG (*7*) and the Mira period-luminosity relation (*8*), we adopt the distance $D = 2.7$ kpc, estimated as the mean derived from photometry in three near-infrared bands, assuming an extinction $E_{B-V} = 0.57$ (*2*).

A nova outburst from V407 Cyg was detected on 10 March 2010 (*9*); it had a magnitude of ~6.9 in an unfiltered charge-coupled device image obtained at 19:08 UT. Subsequent densely sampled observations show that the outburst was followed by a smooth decay, though the precise epoch of the nova is formally uncertain by up to 3 days, due to the time gap from the pre-outburst image (Fig. 1). Monitoring of the source over the past 2 years indicates pre-outburst magnitude values in the range of 9 to 12 [see the supporting online material (SOM)]. V407 Cyg has been monitored optically for decades and has shown earlier signs of optical brightening on month-long time scales by one to two magnitudes in the B and V bands (around 1936 and 1998) from typical V-band magnitudes of 13 to 16 (*2*, *10*, *11*), but the magnitude of the recent nova was unprecedented.

Here, we report on a high-energy γ-ray source (Fig. 2) positionally coincident with V407 Cyg detected after the nova (*12*) during routine automated processing of all-sky monitoring data from the Fermi Large Area Telescope (LAT) (*13*). A γ-ray light curve (1-day time bins) of this source generated from an analysis of all LAT data reveals that the first significant detection (4.3σ) was, in fact, on 10 March, indicating that the γ-ray activity began on the same day as the reported optical maximum of V407 Cyg (Fig. 1; see also SOM). The observed 10 March flux is up to a factor of 3 larger than the 1-day upper limits (unless otherwise noted, 95% confidence limits are reported throughout) on the pre-outburst days. To further isolate the onset of detectable γ-ray emission, we divided the 10 March data into 6-hour intervals,

*All authors with their affiliations appear at the end of this paper.
†To whom correspondence should be addressed. E-mail: Teddy.Cheung.ctr@nrl.navy.mil (C.C.C.); Adam.Hill@obs.ujf-grenoble.fr (A.B.H.); Pierre.Jean@cesr.fr (P.J.); srazzaque@ssd5.nrl.navy.mil (S.R.); Kent.Wood@nrl.navy.mil (K.S.W.)

and the first indication of a signal was a marginal detection in the 12- to 18-hour bin (2.8σ). This was followed by a highly significant detection (at 5.7σ) in the last 6-hours bin (18 to 24 hours), which had a peak flux that was a factor of ≳3 larger than that of the marginal detection and the limits from earlier in the day (see SOM). The initial detection of the γ-ray source by the Fermi-LAT in the latter 12 hours of 10 March is consistent with the time of the optical nova discovery.

The peak flux in γ-rays (defined in 1-day segments) was observed between 13 to 14 March, 3 to 4 days after the initial γ-ray detection, and with a flux (9×10^{-7} photons cm^{-2} s^{-1}) that was greater than that observed on 10 March by a factor of 2. The data was analyzed up to mid-April, and the last day with a significant detection (>3σ) of the variable γ-ray source was 25 March, amounting to a total lifetime of activity of 2 weeks. Defining an "active" period (*14*) from 10 March 18:00 to 29 March 00:00, we obtained a γ-ray position (Fig. 2) from the cumulative exposure that is 0.040° offset from the optical position of V407 Cyg, which is within the LAT 95% confidence circle (radius = 0.062°). The average spectral energy distribution (SED) of the Fermi-LAT γ-ray source during the defined active period can be described with an exponentially cut-off power-law model (see SOM) with a flux (>100 MeV) of $(4.4 \pm 0.4) \times 10^{-7}$ photons cm^{-2} s^{-1} (and an overall source significance of 18.1σ). A likelihood-ratio test indicates that the addition of the exponential cut-off improves the fit at the 4.9σ level compared with a simpler single–power-law model. We find no evidence for spectral variability over the duration of the active γ-ray period (see SOM). Our analysis of the data from the 2 weeks after the active period (29 March to 12 April) collectively gives a significance of only 1.6σ (and a flux upper limit of 0.8×10^{-7} photons cm^{-2} s^{-1}), indicating that the flux has declined below the level of detectability. Overall, the γ-ray source is brightest at earlier times, consistent with the optical behavior of V407 Cyg. The coincident localization and the observed correlated variability imply that the optical nova is the source of the variable γ-ray flux.

Nuclear γ-ray lines and continuum emission from novae at ≲1-MeV energies have been considered (*15*), but the Fermi-LAT detection of V407 Cyg shows unequivocally that novae can generate high-energy (>100 MeV) γ-rays. The >100-MeV γ-ray luminosity, its spectrum, and its light curve can be understood broadly as consequences of shock acceleration taking place in a nova shell. Such a nova shell is produced by thermonuclear energy release on the WD and initially expands freely into a very dense medium consisting of the RG wind and atmosphere present in the binary system prior to the nova. The radio source detected from V407 Cyg over 22 to 28 March (*16*, *17*) and subsequent imaging, which revealed the emission to be predominantly extended at a few milli–arc seconds resolution (*18*), is consistent with a picture of an extended shell, as was found in the 2006 RS Ophiuchi nova outburst (*19*, *20*).

An initially spherical shell can sweep up mass from the companion RG wind asymmetrically and will reach a deceleration phase during which it expands adiabatically (*21*) with different temporal behavior in different directions from the WD center. Fermi acceleration of protons and electrons takes place in the outgoing nova shock during both the free-expansion and deceleration phases, and we show that the measured γ-ray spectrum can be explained by π^0 decay γ-rays from proton-proton (pp) collisions or inverse Compton (IC) scattering of infrared photons from the RG by electrons. In both of these scenarios, the γ-ray light curve, in conjunction with the delayed rise of the x-ray flux, can be explained qualitatively as a geometrical effect of the nova-shell evolution.

The measured optical peak magnitude of 7 of V407 Cyg (*9*) over 1 day implies an energy release of $\gtrsim 3 \times 10^{42}$ ergs at visible frequencies (after extinction correction). The kinetic energy of the ejecta in the nova shell, $\varepsilon_k \sim 10^{44}$ ergs, can be estimated assuming a nova-shell mass $M_{ej} \sim 10^{-6} M_\odot$ [which is a plausible value for a massive WD > $1.25 M_\odot$ (*22*, *23*), where $M_\odot$ is the mass of the Sun] and the velocity $v_{ej} = 3200 \pm 345$ km s^{-1}, inferred from an Hα atomic emission line-width measurement on 14 March (see SOM). The velocity of the outgoing shock wave is initially $v_{sh} \sim v_{ej}$. The onset of the deceleration phase and subsequent evolution of the shock wave are determined by the density of the RG stellar wind and atmosphere surrounding the nova shell, which depend on two poorly constrained parameters: (i) the WD-RG separation (a) and (ii) the RG mass-loss rate in the wind ($\dot{M}_W$). As we will discuss shortly, the detection of the γ-ray flux within 1 day of the optical detection of the nova, a peak duration of 3 to 4 days, and subsequent decay within 15 days after the optical nova can be modeled as emission from the nova shell in a dense environment and

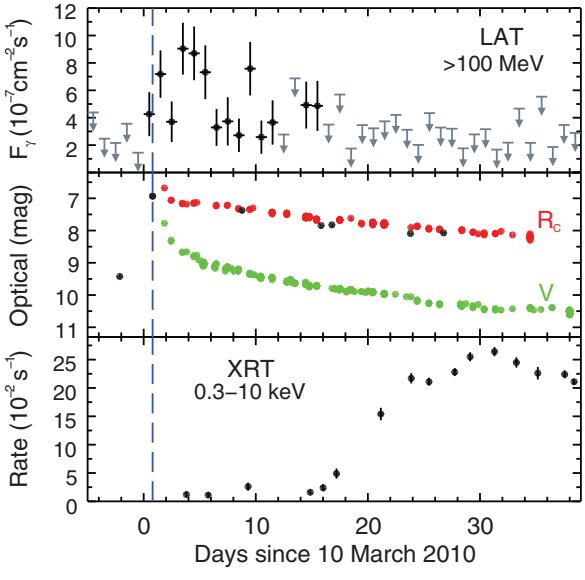

Fig. 1. Light curves of V407 Cyg in γ-rays from the Fermi-LAT (**top**), optical (**middle**), and x-rays from Swift (**bottom**). Vertical bars indicate 1σ statistics errors for all data (the errors are smaller than the points in the optical section). For the γ-ray data, gray arrows indicate 2σ upper limits, and horizontal bars indicate the 1-day binning. In the optical section, unfiltered (black), R_C (red), and V (green) band magnitudes are shown (see SOM). The vertical dashed blue line indicates the epoch of the optical nova detection; the γ-ray peak occurred 3 to 4 days later. $F\gamma$, γ-ray flux; XRT, Swift X-ray Telescope.

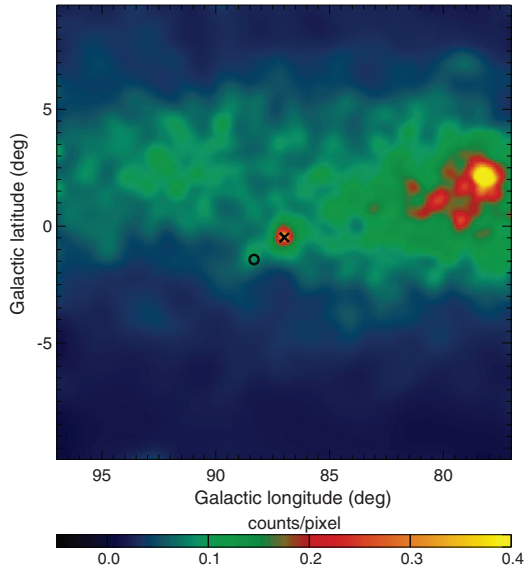

Fig. 2. Fermi-LAT γ-ray counts (200 MeV to 100 GeV) map from 10 March 18:00 to 29 March 00:00 2010 in the region around the position of the γ-ray nova source V407 Cyg (marked by the black cross) at Galactic longitude l = 86.958°, Galactic latitude b = −0.513° (right ascension = 315.551°, declination = +45.737°, J2000.0). The map was adaptively smoothed by imposing a minimum signal-to-noise ratio of 7. The closest known γ-ray source is contained in the first-year LAT catalog (1FGL J2111.3+4607; marked by the black circle) (*29*), ~1.5° away from the star's optical position. The bright source at l = 78.2°, b = +2.1° is LAT PSR J2021+4026. deg, degrees.

mostly from along the WD-RG axis, assuming an inverse-square law wind-density profile from the RG center, with $a \sim 10^{14}$ cm and $\dot{M}_W \sim 3 \times 10^{-7} M_\odot$ year^{-1}. Both of these values are a factor ≈ 2 smaller than those suggested previously for the V407 Cyg system (*2*).

The density of particles in the RG wind is $n(R) = \dot{M}_W [4\pi(R^2 + a^2 - 2aR\cos\theta) v_W \overline{m}]^{-1}$. Here, the RG wind velocity, $v_w \approx 10$ km s^{-1}, is based on optical spectra (see SOM), the mean particle mass is $\overline{m} \approx 10^{-24}$ g, R is the distance from the WD center, and θ is the polar angle relative to the WD center. The energy density in the RG radiation field is, similarly, $u_{IR}(R) = L_{IR}[4\pi(R^2 + a^2 - 2aR\cos\theta)c]^{-1}$, where c is the speed of light. The RG luminosity, $L_{IR} \approx 10^4 L_\odot$ (where $L_\odot$ is the luminosity of the Sun) (*2*, *11*), is consistent with a spectral fit to post-nova infrared measurements with a temperature of ≈ 2500 K (see SOM). Near the WD surface ($R \approx 0.01 R_\odot$, where $R_\odot$ is the radius of the Sun), these densities are $n \sim 10^8$ cm^{-3} and $u_{IR} \sim 0.01$ erg cm^{-3}, and they increase by up to one order of magnitude when the nova shell approaches the RG surface (that is, along θ ≈ 0°) at a radius $r_{RG} \approx 500\ R_\odot$. An equipartition of the energy density in the magnetic field expected to arise from turbulent motions in the wind to the thermal energy density in the RG wind with temperature $T_w \approx 700$ K (*2*) gives a mean magnetic field $B_{sh}(R) = [32\pi n(R) k T_w]^{1/2} \sim 0.03$ G (here, k is the Boltzmann constant) in the shock wave when it is near the WD. Electrons and protons can be accelerated efficiently in this magnetic field (*24*) and interact with the surrounding RG wind particles and radiation.

The time scale for pp interactions for a π^0 model to produce γ-rays in the shock wave is $t_{pp} \approx 1/[4n(R)c\sigma_{pp}] \sim 2.8 \times 10^6$ s when the nova shell is near the WD. Here, $\sigma_{pp} \approx 3 \times 10^{-26}$ cm^2 is the pp cross section. Thus, $t/t_{pp} \sim 3\%$ of the protons can interact to produce π^0 emission on a time scale $t = 1$ day. In an IC scenario, the cooling time scale for electrons with energy $E_e \approx 5$ GeV that upscatter 2500-K photons to ≈ 100 MeV is $t_{IC} = (3/4) m_e^2 c^3 [\sigma_T E_e u_{IR}(R)]^{-1} \sim 3.1 \times 10^5$ s (here, m_e is the mass of the electron, and σ_T is the Thomson electron scattering cross section). Thus, $t/t_{IC} \sim 28\%$ of the electrons produce γ-rays efficiently in a time scale $t = 1$ day. The efficiency for γ-ray production in both the π^0 and IC models increases substantially in the part of the nova shell that expands toward the RG (θ ~ 0°) and reaches the deceleration phase, by accumulating RG wind and atmospheric material of mass equal to M_{ej}, at a distance ~ 7×10^{13} cm in ~2.5 days. The efficiency decreases rapidly in the part of the shell that expands away from the RG (θ ≥ 90°) because of a decreasing density in both the RG wind and radiation.

In our scenario, most of the γ-rays come from the part of the nova shell approaching the RG. This can qualitatively explain the basic features of the γ-ray light curve (Fig. 1): (i) its onset within days of the optical nova and the peak flux reached in 3 days due to an increasing efficiency for pp interactions and an increasing volume of the shock-accelerated particles and (ii) the decline in the flux after ~5 days due to weakening of the shock wave after reaching the deceleration phase. A highly significant 1-day detection (6.5σ) of an increase in γ-ray flux 9 days after the nova discovery (Fig. 1) could be due to the nova shell hitting a part of the RG surface or a nearby remnant of high density with a size scale of $\sim 10^{13} (v_{sh}/1500\ \text{km s}^{-1})(t/1\ \text{day})$ cm.

A representative π^0 decay model fitting the LAT data with a cosmic-ray proton spectrum in the form of an exponentially cut-off power-law $N_p = N_{p,0}(W_p + m_p c^2)^{-s_p} e^{-W_p/E_{cp}}$ (where E_{cp}, W_p, and m_p are the cut-off energy, kinetic energy, and mass of the proton, respectively) is shown in Fig. 3. The γ-ray spectrum is well reproduced with a spectral index $s_p = 2.15^{+0.45}_{-0.28}$, similar to the expected spectrum from the Fermi acceleration mechanism, with $E_{cp} = 32^{+85}_{-8}$ GeV (1σ uncertainties) (see SOM). The total energy in γ-rays above 100 MeV integrated over the active period is $\varepsilon_\gamma \approx 3.6 \times 10^{41}$ erg. The total energy in protons is $\varepsilon_p \approx \in_p^{-1} \langle E_p/E_\gamma \rangle \varepsilon_\gamma$, where $\in_p$ is the mean efficiency for pp interactions and $1/\langle E_p/E_\gamma \rangle \approx 0.2$ is the mean fraction of proton energy transfer to γ-rays per interaction in the $E_\gamma \geq 100$ MeV range. The ratio of the total energy in protons that produce γ-rays to the kinetic energy ($\varepsilon_p/\varepsilon_k \sim 9\%$), with $\in_p \sim 0.2$ averaged over the γ-ray source lifetime of 15 days and the whole nova shell, is similar to 1 to 10% estimated in supernova remnants (*25*). The ratio, however, is larger when considering dominant γ-ray emission coming mostly from the part of the shell that expands toward the RG.

The leptonic model is represented in Fig. 3 as the total of the IC spectrum plus a small contribution from bremsstrahlung emission that arises from the scattering of electrons with protons of density $n(R)$ in the shock wave (see SOM). The exponentially cut-off power-law electron spectrum, $N_e = N_{e,0} W_e^{-s_e} e^{-W_e/E_{ce}}$, where E_{ce} and W_e are the cut-off energy and kinetic energy of electrons (in billion electron volts), respectively, reproduces the γ-ray spectrum with a spectral index $s_e = -1.75^{+2.40}_{-0.59}$ and $E_{ce} = 3.2^{+2.6}_{-0.1}$ GeV (1σ uncertainties) (see SOM). The total number of electrons emitting in the steady state is $N_{e,0} \approx 4 \times 10^{42}$ electrons, with a mean energy of 8.7 GeV, which is larger than E_{ce} because of the steep spectrum. The total energy in electrons over 15 days of γ-ray emission is $\varepsilon_e \approx 4 \times 10^{41}$ ergs, averaged over the nova shell. Thus, the total energy in electrons that produce γ-rays in the IC model is a small fraction of the kinetic energy in the shell ($\varepsilon_e/\varepsilon_k \sim 0.4\%$).

X-ray emission detected from V407 Cyg with the Swift X-ray Telescope as early as 3 days after the onset of the optical nova (Fig. 1) is probably due to shock-heating of ambient gas (*26*, *27*). The x-ray flux starts rising substantially about 2 weeks after the nova, coinciding with when the γ-ray flux declines below the level of detectability. In our geometric scenario, the sharply rising x-ray flux is due to the increasing volume of shocked gas in the nova shell expanding in the direction away from the RG. The x-ray flux peaks about 30 days after the explosion, and its subsequent slow decline is consistent with the longer time scale of the deceleration phase.

The Fermi-LAT detection of V407 Cyg was a surprise and adds novae as a source class to the high-energy γ-ray sky. The particle acceleration mechanism and the γ-ray emission scenarios outlined here require the mass donor to be a RG; that is, a nova in a symbiotic system. Interestingly, several symbiotic stars are known to be recurrent novae (i.e., systems observed to have undergone multiple thermonuclear runaways within the last century), and recurrent novae are often considered candidate progenitors of type Ia supernovae (*28*). V407 Cyg may also belong to this class of binaries, and we have adopted parameters that are consistent with such a classification in modeling the γ-ray emission. In general, these sources can have dramatic influence on the local interstellar medium and Galactic cosmic rays, but few binary systems with a WD are known to have a similar environment; hence, we expect γ-ray novae to be rare.

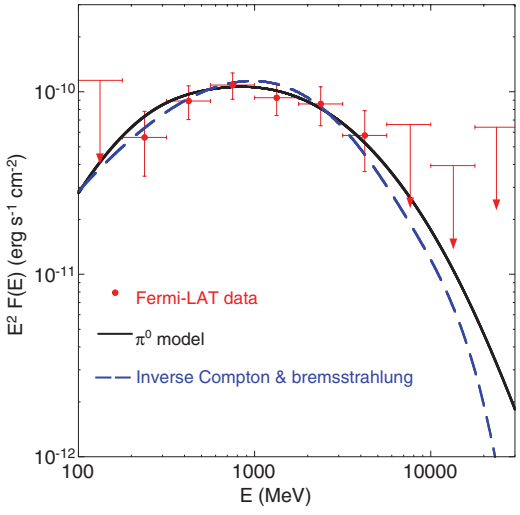

Fig. 3. SED of V407 Cyg in million electron volt/billion electron volt γ-rays measured by the Fermi-LAT instrument over the period from 10 March 18:00 to 29 March 00:00 2010. Vertical bars indicate 1σ statistical errors, red arrows indicate 2σ upper limits, and horizontal bars indicate energy ranges. The best-fit π^0 (black solid line) and leptonic (blue dashed line) models are indicated.

References and Notes

1. S. J. Kenyon, in *Evolutionary Processes in Interacting Binary Stars*, Y. Kondo *et al.*, Eds., International Astronomical Union (IAU) Symposium, vol. 151 (IAU, Kluwer Academic, Dordrecht, Netherlands, 1992), p. 137.
2. U. Munari, R. Margoni, R. Stagni, *Mon. Not. R. Astron. Soc.* **242**, 653 (1990).
3. S. Deguchi, J.-I. Nakashima, T. Miyata, Y. Ita, *Publ. Astron. Soc. Jpn.* **57**, 933 (2005).
4. R. J. Ivison, E. R. Seaquist, P. J. Hall, *Mon. Not. R. Astron. Soc.* **269**, 218 (1994).
5. S. Y. Shugarov, A. A. Tatarnikova, E. A. Kolotilov, V. I. Shenavrin, B. F. Yudin, *Balt. Astron.* **16**, 23 (2007).
6. A. A. Tatarnikova *et al.*, *Mon. Not. R. Astron. Soc.* **344**, 1233 (2003).
7. L. Meinunger, *Mitt. Veranderl. Sterne.* **87**, 111 (1966).
8. I. S. Glass, M. W. Feast, *Mon. Not. R. Astron. Soc.* **199**, 245 (1982).
9. K. Nishiyama, F. Kabashima, International Astronomical Union Central Bureau for Astronomical Telegrams, reported by H. Maehara, no. 2199 (2010).
10. C. Hoffmeister, *Veröff. Sternw. Sonneberg.* **1**, 295 (1949).
11. E. A. Kolotilov, V. I. Shenavrin, S. Y. Shugarov, B. F. Yudin, *Astron. Rep.* **47**, 777 (2003).
12. C. C. Cheung *et al.*, Fermi-LAT Collaboration, *The Astronomer's Telegram* **2487**, 1 (2010).
13. W. B. Atwood *et al.*, *Astrophys. J.* **697**, 1071 (2009).
14. The window was extended by 3 days to include any late low-level emission that would not be detectable on any individual daily bin.
15. M. Hernanz, in *Classical Novae*, M. F. Bode, A. Evans, Eds. (Cambridge Univ. Press, Cambridge, ed. 2, 2008) p. 252.
16. I. Nestoras *et al.*, *The Astronomer's Telegram* **2506**, 1 (2010).
17. G. C. Bower, R. Forster, C. C. Cheung, *The Astronomer's Telegram* **2529**, 1 (2010).
18. M. Giroletti *et al.*, *The Astronomer's Telegram* **2536**, 1 (2010).
19. T. J. O'Brien *et al.*, *Nature* **442**, 279 (2006).
20. M. P. Rupen, A. J. Mioduszewski, J. L. Sokoloski, *Astrophys. J.* **688**, 559 (2008).
21. L. I. Sedov, *Similarity and Dimensional Methods in Mechanics* (Academic Press, New York, 1959).
22. S. Starrfield, W. M. Sparks, J. W. Truran, M. C. Wiescher, *Astrophys. J.* **127** (suppl.), 485 (2000).
23. O. Yaron, D. Prialnik, M. M. Shara, A. Kovetz, *Astrophys. J.* **623**, 398 (2005).
24. V. Tatischeff, M. Hernanz, *Astrophys. J.* **663**, L101 (2007).
25. A. A. Abdo *et al.*, *Astrophys. J.* **710**, L92 (2010).
26. J. L. Sokoloski, G. J. M. Luna, K. Mukai, S. J. Kenyon, *Nature* **442**, 276 (2006).
27. J. J. Drake *et al.*, *Astrophys. J.* **691**, 418 (2009).
28. W. M. Wood-Vasey, J. L. Sokoloski, *Astrophys. J.* **645**, L53 (2006).
29. A. A. Abdo *et al.*, *Astrophys. J.* **188** (suppl.), 405 (2010).

30. The Fermi-LAT Collaboration acknowledges support from a number of agencies and institutes for both the development and operation of the LAT, as well as for scientific data analysis. These organizations include NASA and the U.S. Department of Energy in the United States; CEA/Irfu and IN2P3/CNRS in France; ASI and Istituto Nazionale de Fisica Nucleare in Italy; Ministry of Education, Culture, Sports, Science and Technology (MEXT), High Energy Accelerator Research Organization (KEK), and JAXA in Japan; and the K. A. Wallenberg Foundation, the Swedish Research Council, and the National Space Board in Sweden. We also gratefully acknowledge additional support from INAF in Italy and the Centre National d'Etudes Spatiales in France for science analysis during the operations phase. We acknowledge with thanks the variable star observations from the American Association of Variable Star Observers International Database contributed by observers worldwide and used in this research. J. Conrad is a Royal Swedish Academy of Sciences Research Fellow, funded by a grant from the K. A. Wallenberg Foundation; G.D. and A.B.H. were funded by contract ERC-StG-200911 from the European Community; P.K. was supported by the Astronomical Institute, Academy of Sciences of the Czech Republic (Ondrejov, Czech Republic); and L.T. was partially supported by the International Doctorate on Astroparticle Physics program.

The Fermi-LAT Collaboration

A. A. Abdo,[1,2] M. Ackermann,[3] M. Ajello,[3] W. B. Atwood,[4] L. Baldini,[5] J. Ballet,[6] G. Barbiellini,[7,8] D. Bastieri,[9,10] K. Bechtol,[3] R. Bellazzini,[5] B. Berenji,[3] R. D. Blandford,[3] E. D. Bloom,[3] E. Bonamente,[11,12] A. W. Borgland,[3] A. Bouvier,[3] T. J. Brandt,[13,14] J. Bregeon,[5] A. Brez,[5] M. Brigida,[15,16] P. Bruel,[17] R. Buehler,[3] T. H. Burnett,[18] S. Buson,[9,10] G. A. Caliandro,[19] R. A. Cameron,[3] P. A. Caraveo,[20] S. Carrigan,[10] J. M. Casandjian,[6] C. Cecchi,[11,12] Ö. Çelik,[21,22,23] E. Charles,[3] S. Chaty,[6] A. Chekhtman,[1,24] C. C. Cheung,[1,2]† J. Chiang,[3] S. Ciprini,[12] R. Claus,[3] J. Cohen-Tanugi,[25] J. Conrad,[26,27] S. Corbel,[6,28] R. Corbet,[21,23] M. E. DeCesar,[21,29] P. R. den Hartog,[3] C. D. Dermer,[1] F. de Palma,[15,16] S. W. Digel,[3] D. Donato,[22,29] E. do Couto e Silva,[3] P. S. Drell,[3] R. Dubois,[3] G. Dubus,[30] D. Dumora,[31,32] C. Favuzzi,[15,16] S. J. Fegan,[17] E. C. Ferrara,[21] P. Fortin,[17] M. Frailis,[33,34] L. Fuhrmann,[35] Y. Fukazawa,[36] S. Funk,[3] P. Fusco,[15,16] F. Gargano,[16] D. Gasparrini,[37] N. Gehrels,[21] S. Germani,[11,12] N. Giglietto,[15,16] F. Giordano,[15,16] M. Giroletti,[39] T. Glanzman,[3] G. Godfrey,[3] I. A. Grenier,[6] M.-H. Grondin,[31,32] J. E. Grove,[1] S. Guiriec,[39] D. Hadasch,[40] A. K. Harding,[21] M. Hayashida,[3] E. Hays,[21] S. E. Healey,[3] A. B. Hill,[30]† D. Horan,[17] R. E. Hughes,[14] R. Itoh,[36] P. Jean,[13]† G. Jóhannesson,[3] A. S. Johnson,[3] R. P. Johnson,[4] T. J. Johnson,[21,29] W. N. Johnson,[1] T. Kamae,[3] H. Katagiri,[36] J. Kataoka,[41] M. Kerr,[18] J. Knödlseder,[13] E. Koerding,[6] M. Kuss,[5] J. Lande,[3] L. Latronico,[5] S.-H. Lee,[3] M. Lemoine-Goumard,[31,32] M. Llena Garde,[26,27] F. Longo,[7,8] F. Loparco,[15,16] B. Lott,[31,32] M. N. Lovellette,[1] P. Lubrano,[11,12] A. Makeev,[1,24] M. N. Mazziotta,[16] W. McConville,[21,29] J. E. McEnery,[21,29] J. Mehault,[25] P. F. Michelson,[3] T. Mizuno,[36] A. A. Moiseev,[22,29] C. Monte,[15,16] M. E. Monzani,[3] A. Morselli,[42] I. V. Moskalenko,[3] S. Murgia,[3] T. Nakamori,[41] M. Naumann-Godo,[6] I. Nestoras,[35] P. L. Nolan,[3] J. P. Norris,[43] E. Nuss,[25] M. Ohno,[44] T. Ohsugi,[45] A. Okumura,[44] N. Omodei,[3] E. Orlando,[46] J. F. Ormes,[43] M. Ozaki,[44] D. Paneque,[3] J. H. Panetta,[3] D. Parent,[1,24] V. Pelassa,[25] M. Pepe,[11,12] M. Pesce-Rollins,[5] F. Piron,[25] T. A. Porter,[3] S. Rainò,[15,16] R. Rando,[9,10] P. S. Ray,[1] M. Razzano,[5] S. Razzaque,[1,2]† N. Rea,[19] A. Reimer,[47,3] O. Reimer,[47,3] T. Reposeur,[31,32] J. Ripken,[26,27] S. Ritz,[4] R. W. Romani,[3] M. Roth,[18] H. F.-W. Sadrozinski,[4] A. Sander,[14] P. M. Saz Parkinson,[4] J. D. Scargle,[48] F. K. Schinzel,[35] C. Sgrò,[5] M. S. Shaw,[3] E. J. Siskind,[49] D. A. Smith,[31,32] P. D. Smith,[14] K. V. Sokolovsky,[35,50] G. Spandre,[5] P. Spinelli,[15,16] Ł. Stawarz,[44,51] M. S. Strickman,[1] D. J. Suson,[52] H. Takahashi,[45] T. Takahashi,[44] T. Tanaka,[3] Y. Tanaka,[44] J. B. Thayer,[3] J. G. Thayer,[3] D. J. Thompson,[21] L. Tibaldo,[9,10,6] D. F. Torres,[19,40] G. Tosti,[11,12] A. Tramacere,[3,53,54] Y. Uchiyama,[3] T. L. Usher,[3] J. Vandenbroucke,[3] V. Vasileiou,[22,23] N. Vilchez,[13] V. Vitale,[42,55] A. P. Waite,[3] E. Wallace,[18] P. Wang,[3] B. L. Winer,[14] M. T. Wolff,[1] K. S. Wood,[1]† Z. Yang,[26,27] T. Ylinen,[56,57,27] M. Ziegler,[4] H. Maehara,[58] K. Nishiyama,[59] F. Kabashima,[59] U. Bach,[35] G. C. Bower,[60] A. Falcone,[61] J. R. Forster,[60,62] A. Henden,[63] K. S. Kawabata,[45] P. Koubsky,[64] K. Mukai,[21,23] T. Nelson,[21,23] S. R. Oates,[65] K. Sakimoto,[36] M. Sasada,[36] V. I. Shenavrin,[66] S. N. Shore,[5,67] G. K. Skinner,[22,29] J. Sokoloski,[68] M. Stroh,[59] A. M. Tatarnikov,[66] M. Uemura,[45] G. M. Wahlgren,[69,21] M. Yamanaka[36]

[1]Space Science Division, Naval Research Laboratory, Washington, DC 20375, USA. [2]National Research Council Research Associate, National Academy of Sciences, Washington, DC 20001, USA. [3]W. W. Hansen Experimental Physics Laboratory, Kavli Institute for Particle Astrophysics and Cosmology, Department of Physics and SLAC National Accelerator Laboratory, Stanford University, Stanford, CA 94305, USA. [4]Santa Cruz Institute for Particle Physics, Department of Physics and Department of Astronomy and Astrophysics, University of California at Santa Cruz, Santa Cruz, CA 95064, USA. [5]Istituto Nazionale di Fisica Nucleare, Sezione di Pisa, I-56127 Pisa, Italy. [6]Laboratoire AIM, CEA-IRFU/CNRS/Université Paris Diderot, Service d'Astrophysique, CEA Saclay, 91191 Gif sur Yvette, France. [7]Istituto Nazionale di Fisica Nucleare, Sezione di Trieste, I-34127 Trieste, Italy. [8]Dipartimento di Fisica, Università di Trieste, I-34127 Trieste, Italy. [9]Istituto Nazionale di Fisica Nucleare, Sezione di Padova, I-35131 Padova, Italy. [10]Dipartimento di Fisica "G. Galilei," Università di Padova, I-35131 Padova, Italy. [11]Istituto Nazionale di Fisica Nucleare, Sezione di Perugia, I-06123 Perugia, Italy. [12]Dipartimento di Fisica, Università degli Studi di Perugia, I-06123 Perugia, Italy. [13]Centre d'Étude Spatiale des Rayonnements, CNRS/UPS, BP 44346, F-30128 Toulouse Cedex 4, France. [14]Department of Physics, Center for Cosmology and Astro-Particle Physics, The Ohio State University, Columbus, OH 43210, USA. [15]Dipartimento di Fisica "M. Merlin" dell'Università e del Politecnico di Bari, I-70126 Bari, Italy. [16]Istituto Nazionale di Fisica Nucleare, Sezione di Bari, 70126 Bari, Italy. [17]Laboratoire Leprince-Ringuet, École polytechnique, CNRS/IN2P3, Palaiseau, France. [18]Department of Physics, University of Washington, Seattle, WA 98195–1560, USA. [19]Institut de Ciencies de l'Espai (IEEC-CSIC), Campus UAB, 08193 Barcelona, Spain. [20]Istituto Nazionale di Astrofisica (INAF)–Istituto di Astrofisica Spaziale e Fisica Cosmica, I-20133 Milano, Italy. [21]NASA Goddard Space Flight Center, Greenbelt, MD 20771, USA. [22]Center for Research and Exploration in Space Science and Technology and NASA Goddard Space Flight Center, Greenbelt, MD 20771, USA. [23]Department of Physics and Center for Space Sciences and Technology, University of Maryland Baltimore County, Baltimore, MD 21250, USA. [24]George Mason University, Fairfax, VA 22030, USA. [25]Laboratoire de Physique Théorique et Astroparticules, Université Montpellier 2, CNRS/IN2P3, Montpellier, France. [26]Department of Physics, Stockholm University, AlbaNova, SE-106 91 Stockholm, Sweden. [27]The Oskar Klein Centre for Cosmoparticle Physics, AlbaNova, SE-106 91 Stockholm, Sweden. [28]Institut universitaire de France, 75005 Paris, France. [29]Department of Physics and Department of Astronomy, University of Maryland, College Park, MD 20742, USA. [30]Université Joseph Fourier–Grenoble 1/CNRS, laboratoire d'Astrophysique de Grenoble UMR 5571, BP 53, 38041 Grenoble Cedex 09, France. [31]CNRS/IN2P3, Centre d'Études Nucléaires Bordeaux Gradignan, UMR 5797, Gradignan, 33175, France. [32]Université de Bordeaux, Centre d'Études Nucléaires Bordeaux Gradignan, UMR 5797, Gradignan, 33175, France. [33]Dipartimento di Fisica, Università di Udine and Istituto Nazionale di Fisica Nucleare, Sezione di Trieste, Gruppo Collegato di Udine, I-33100 Udine, Italy. [34]Osservatorio Astronomico di Trieste, Istituto Nazionale di Astrofisica, I-34143 Trieste, Italy. [35]Max-Planck-Institut für Radioastronomie, Auf dem Hügel 69, 53121 Bonn, Germany. [36]Department of Physical Sciences, Hiroshima University, Higashi-Hiroshima, Hiroshima 739-8526, Japan. [37]Agenzia Spaziale Italiana (ASI) Science Data Center, I-00044 Frascati (Roma), Italy. [38]INAF Istituto di Radioastronomia, 40129 Bologna, Italy. [39]Center for Space Plasma and Aeronomic Research, University of Alabama in Huntsville, Huntsville, AL 35899, USA. [40]Institució Catalana de Recerca i Estudis Avançats, Barcelona, Spain. [41]Research Institute for Science and Engineering, Waseda University, 3-4-1, Okubo, Shinjuku, Tokyo, 169-8555 Japan. [42]Istituto Nazionale di Fisica Nucleare, Sezione di Roma "Tor Vergata," I-00133 Roma, Italy. [43]Department of Physics and Astronomy, University of Denver, Denver, CO 80208, USA. [44]Institute of Space and Astronautical Science, Japanese Aerospace Exploration Agency (JAXA), 3-1-1 Yoshinodai, Sagamihara, Kanagawa 229-8510, Japan. [45]Hiroshima Astrophysical Science Center, Hiroshima University, Higashi-Hiroshima, Hiroshima 739-8526, Japan. [46]Max-Planck Institut für extraterrestrische Physik, 85748 Garching, Germany. [47]Institut für Astro- und Teilchenphysik and Institut für Theoretische Physik, Leopold-Franzens-Universität Innsbruck, A-6020 Innsbruck, Austria. [48]Space Sciences Division, NASA Ames Research Center, Moffett Field, CA 94035–1000, USA. [49]NYCB Real-Time Computing, Lattingtown, NY 11560–1025, USA. [50]Astro Space Center of the Lebedev Physical Institute, 117810 Moscow, Russia. [51]Astronomical Observatory, Jagiellonian University, 30-244 Kraków, Poland. [52]Department of Chemistry and Physics, Purdue University Calumet, Hammond, IN 46323–2094, USA. [53]Consorzio Interuniversitario per la Fisica Spaziale, I-10133 Torino, Italy. [54]INTEGRAL Science Data Centre, CH-1290 Versoix, Switzerland. [55]Dipartimento di Fisica, Università di Roma "Tor Vergata," I-00133 Roma, Italy. [56]Department of Physics, Royal Institute of Technology, AlbaNova, SE-106 91 Stockholm, Sweden. [57]School of Pure and Applied Natural Sciences, University of Kalmar, SE-391 82 Kalmar, Sweden. [58]Kwasan and Hida Observatories, Kyoto University, Kyoto 607-8471, Japan. [59]Miyaki-Argenteus Observatory, Miyaki-cho, Saga-ken, Japan. [60]Department of Astronomy, University of California, Berkeley, CA 94720–3411, USA. [61]Department of Astronomy and Astrophysics, Pennsylvania State University, University Park, PA 16802, USA. [62]Hat Creek Observatory, Hat Creek, CA 96040, USA. [63]American

Association of Variable Star Observers, Cambridge, MA 02138, USA. [64]Astronomical Institute, Academy of Sciences of the Czech Republic, Ondrejov, Czech Republic. [65]Mullard Space Science Laboratory, University College London, Holmbury St. Mary, Dorking, Surrey, RH5 6NT, UK. [66]Sternberg Astronomical Institute, Moscow University, Moscow, Russia. [67]Dipartimento di Fisica "Enrico Fermi," Università di Pisa, Pisa I-56127, Italy. [68]Columbia Astrophysics Laboratory, Columbia University, New York, NY 10027, USA. [69]Catholic University of America, Washington, DC 20064, USA.

Supporting Online Material
www.sciencemag.org/cgi/content/full/329/5993/817/DC1
Materials and Methods
SOM Text
Figs. S1 to S6
Tables S1 to S3
References

19 May 2010; accepted 12 July 2010
10.1126/science.1192537

Quantum Oscillations and Hall Anomaly of Surface States in the Topological Insulator Bi_2Te_3

Dong-Xia Qu,[1]* Y. S. Hor,[2] Jun Xiong,[1] R. J. Cava,[2] N. P. Ong[1]*

Topological insulators are insulating materials that display massless, Dirac-like surface states in which the electrons have only one spin degree of freedom on each surface. These states have been imaged by photoemission, but little information on their transport parameters, for example, mobility, is available. We report the observation of Shubnikov–de Haas oscillations arising from the surface states in nonmetallic crystals of Bi_2Te_3. In addition, we uncovered a Hall anomaly in weak fields, which enables the surface current to be seen directly. Both experiments yield a surface mobility (9000 to 10,000 centimeter^2 per volt-second) that is substantially higher than in the bulk. The Fermi velocity of 4×10^5 meters per second obtained from these transport experiments agrees with angle-resolved photoemission experiments.

Recently, the existence of a new class of bulk insulators called topological insulators has been predicted (*1*–*6*). In a topological insulator, the bulk energy gap is traversed by surface states in which the spin of the electron is locked perpendicular to its momentum by strong spin-orbit interaction. On each surface, the electrons have only one spin degree of freedom (fixed helicity). The spin-resolved nature of the surface states has been confirmed in angle-resolved photoemission spectroscopy (ARPES) experiments on BiSb (*7*), Sb (*8*), Bi_2Se_3 (*9*), and Bi_2Te_3 (*10*). The spin locking in BiSb has also been studied by scanning tunneling microscopy (*11*). However, it has been a challenge to resolve the conductance of the surface states from the dominant bulk contribution (*12*, *13*). The lack of transport information, especially the mobility, is a serious hindrance. Moreover, detection of the surface currents is a crucial first step in the investigation of phenomena, such as the Majorana fermion (*5*) and unconventional electrodynamics (*6*), in topological insulators.

We report dual evidence for surface state conduction in Bi_2Te_3 from Shubnikov–de Haas (SdH) oscillations and from the weak-field Hall effect. As in the case of the selenide Bi_2Se_3 (*12*), as-grown crystals of Bi_2Te_3 usually display a metallic resistivity ρ versus temperature T (in Bi_2Te_3, the Fermi energy E_F lies in the valence band VB). By selective cleaving of many crystals from a boule of Bi_2Te_3 grown with a weak compositional gradient (*14*), we have obtained nonmetallic crystals (Fig. 1A). In the nonmetallic samples Q1, Q2, and Q3, ρ rises when T is lowered below 150 K and saturates to values 4 to 5 mohm cm at 4 K or ~50 times larger than the value in the metallic sample N1. The surface state dispersion obtained by ARPES (*10*) is sketched in Fig. 1B, with E_F in our samples indicated. Even in the most resistive sample Q3, the bulk conductance is ~300 times larger than the surface term (see below). Nonetheless, the latter may be resolved by detecting the SdH oscillations in the resistivity and the Hall resistivity ρ_{yx} at low T. Quantum oscillations are well resolved in the raw trace of the Hall conductivity $\sigma_{xy} = \rho_{yx}/(\rho_{xx}^2 + \rho_{yx}^2)$ measured at $T = 0.3$ K (Fig. 1, C and D). In metals, SdH oscillations correspond to successive emptying of Landau levels (LL) as the magnetic field H is increased. The LL index n is related to the extremal cross section S_F of the Fermi surface (FS) by

$$2\pi(n + \gamma) = S_F \frac{\hbar}{eB} \qquad (1)$$

where $\gamma = 0$ or ½, e is the electron charge, h is Planck's constant ($\hbar = h/2\pi$), and B is the magnetic flux density.

For a two-dimensional (2D) FS, the peak positions depend only on the field component $H_\perp = H\cos\theta$ along the axis **c** normal to the cleavage plane (θ is the tilt angle between **H** and **c**). To

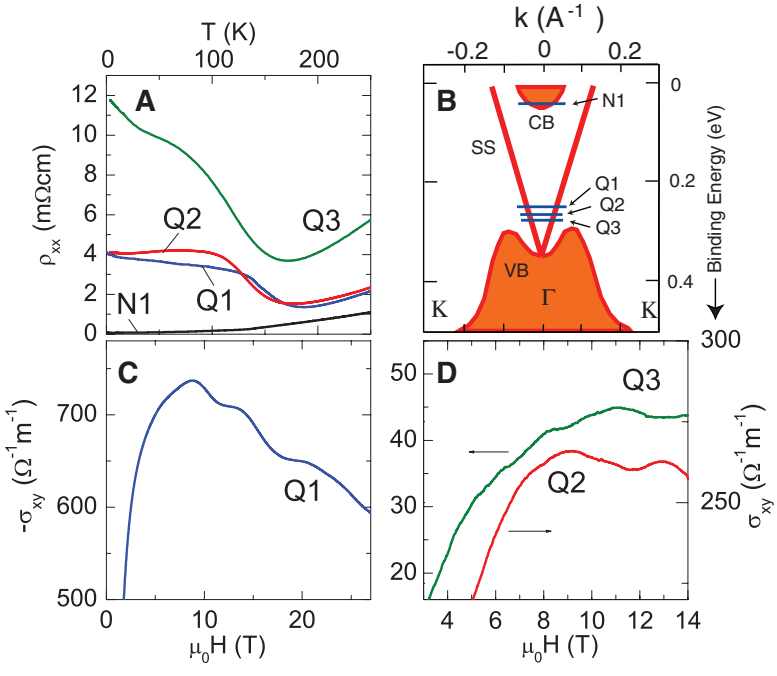

Fig. 1. (**A**) The resistivity profiles ρ versus temperature T of samples Q1, Q2, Q3, and N1. (**B**) Sketch of the surface state dispersion near the Γ point [traced from (*10*)]. The Fermi energies of samples Q1, Q2, Q3, and N1 are indicated by short lines (CB, conduction band). Curves of the Hall conductivity σ_{xy} versus the magnetic field H in sample Q1 (**C**) and in samples Q2 and Q3 (**D**) showing well-resolved SdH oscillations. μ_0 is the permeability.

[1]Department of Physics, Princeton University, Princeton, NJ 08544, USA. [2]Department of Chemistry, Princeton University, Princeton, NJ 08544, USA.

*To whom correspondence should be addressed. E-mail: dqu@princeton.edu (D.-X.Q.); npo@princeton.edu (N.P.O.)